IEEE *Access*

Magnetic Field Sensing Based on Magnetoelectric Coupling of Ampere Force Effect With Piezoelectric Effect in Silver/Poly(Vinylidine Fluoride)/Silver Laminated Composite

BING QI, YUDONG ZHANG[ID], AND TAIPING YAO

Key Laboratory of Modern Power System Simulation and Control and Renewable Energy Technology, Ministry of Education, School of Electrical Engineering, Northeast Electric Power University, Jilin 132012, China

Corresponding author: Yudong Zhang (2684255065@qq.com)

ABSTRACT With the advantages of large piezoelectric constant, wide frequency response range and good flexibility, Poly(vinylidine fluoride) (PVDF) is receiving heightened attention as a promising alternative to traditional piezoelectric materials. This paper focuses on investigating the magnetoelectric effect of a three-layer composite consisting of a core layer of PVDF and two layers of silver-plated electrodes under the action of AC and DC magnetic fields. The resonance frequency of the measurement system is firstly determined to obtain the maximum magnetoelectric response. Then, the existence of magnetoelectric effect in the laminated sample is further verified, which is realized through the coupling of the piezoelectric effect and the Ampere forces caused by the eddy current under the DC bias magnetic field. The experimental results show that the magnetoelectric voltage has an excellent linear response to both AC and DC magnetic fields. The magnetoelectric voltage coefficient is obtained as 299.97 mV/cm·Oe at the resonance frequency under the DC magnetic field of 1000 Oe amplitude. Besides, the theoretical model of the magnetoelectric energy conversion is established, which matches well with the experimental results. Consequently, both AC and DC magnetic field sensing can be realized by observing the magnetoelectric voltage. Without requiring a magnetostrictive phase and power supply, the three-layer composite with a considerable magnetoelectric effect is promising for the application of online monitoring sensors used in the smart grid.

INDEX TERMS Smart grid, magnetoelectric effect, sensor, Poly (vinylidine fluoride) (PVDF), magnetic field detection, eddy current.

I. INTRODUCTION

The smart grid, referred to as the next-generation power system, is regarded as a significant revolution of the traditional power grid. There is no unified concept of the smart grid, but a common agreement has been reached on the crucial requirements for essential energy supply: the efficient and reliable transmission and distribution of electricity [1]–[3]. As we all know, the current power system becomes more and more complicated duo to ever-increasing demand for power supply all over the world. Due to the low popularization of modern technology, traditional power grid suffers from

overload condition, energy loss and slow demand response, which affect the effective supply of electric energy to some extent [4], [5]. By contrast, the smart grid could provide more scientific power management and more accurate electricity distribution on the basis of reasonable statistical analysis of data [6]. In a smart grid scenario, online monitoring of transmission lines and key network nodes is of vital importance, which can effectively improve the reliability of power system. Accurate and real-time information about the state of a power grid can significantly reduce the costs of unexpected outage and the loss of productivity. Comprehensive information drives better decision making: accurate fault diagnosis, rapid demand responses and precise load control [3], [7], [8]. That is, the advanced sensing systems play an important role in the

---

The associate editor coordinating the review of this manuscript and approving it for publication was Jing Liang[ID].

construction of smart grid. Although the traditional sensors (e.g. the Hall devices and the Rogowski coil) can realize the basic function of signal processing, the problems such as continuous power supply and low accuracy are increasingly exposed in practical applications [9], [10]. In this context, new sensing devices based on functional materials with simpler structure, wider rangeability and higher accuracy have emerged as a promising approach to meet the needs of smart grid [11]–[14].

Since 2001, multiferroic magnetoelectric (ME) materials have stimulated a sharply increasing number of research activities due to their potential applications for the multifunctional sensing devices with great design flexibility and high ME conversion efficiency [15], [16]. Ryu *et al.* [17] manufactured magnetostrictive-piezoelectric laminated composites composed of $Pb(Zr,Ti)O_3$ (PZT) and Terfenol-D disks. Experimental results indicated that the ME voltage coefficient increased with decreasing thickness and increasing piezoelectric voltage constant of the PZT layer. The highest ME voltage coefficient they obtained at room temperature rose to 4.68 V/cm·Oe, which was much higher than the previously reported value presented by Ryu*et al.* [17] and Boomgaard and Born [18]. Based on Metglas/PZT/Metglas laminated materials, Bichurin *et al.* [19] designed a ME current sensor which was used to detect the low current in the current-carrying coil. The sensitivity of the ME current sensor at the resonance frequency was 0.53 V/A and the nonlinearity was less than 0.5% when the working range of applied current was 0-5 A. Leung *et al.* [20] investigated the ME effect in a magnetostrictive-piezoelectric composite $(Tb_{0.3}Dy_{0.7}Fe_{1.92}/NdFeB/epoxy/PZT)$. With the advantages of magnetic bias-free and wide bandwidth, the ME sensor they produced in the shape of a concentric ring could achieve a high ME coefficient of 2.77 V/cm·Oe and a linear current sensitivity of 185 mV/A at the resonance frequency. Besides, Zhang *et al.* [21] presented an autonomous current-sensing system consisting of a $SmFe_2/PZT/SmFe_2$ self-biased ME composite and a $Fe_{73.5}Cu_1Nb_3Si_{13.5}B_9$ nanocrystalline flux concentrator for detecting weak current. Experimental results demonstrated that the presented sensor had a linear sensitivity of 152 mV/A at 50 Hz with a slight nonlinearity of 0.01%. However, the above-mentioned ME sensors were all obtained by combining giant magnetostrictive materials and piezoelectric materials. Due to the high manufacturing cost and magnetic hysteresis, giant magnetostrictive materials had great limitations in the wide application of sensors [22]. In particular, Guiffard *et al.* [23] reported on a new ME coupling induced by the eddy current within the silver electrodes of the PZT/silver composite. The ME energy conversion was finally achieved with only a simple piezoelectric unimorph bender, which required no magnetic phase. Compared with the piezoelectric ceramic PZT, the piezoelectric polymer Poly(vinylidine fluoride) (PVDF) had larger piezoelectric voltage constant, smaller dielectric constant and lower elastic modulus, which was considered to have more excellent piezoelectric properties to further strengthen the ME coupling

effect. With the advantages of large piezoelectric constant, wide frequency response range, high mechanical strength and good flexibility, PVDF has been widely applied to the fields of energy collection and sensor monitoring in recent years [24], [25].

The objective of this paper is to discuss the ME coupling effect within a metallic/piezoelectric heterostructure composed of two silver layers coated on the upper and bottom surfaces of a PVDF layer, respectively. By measuring the output voltage versus the frequency of the applied AC magnetic field, the resonance frequency of the measurement system is firstly determined to obtain the maximum ME response. Then, the existence of ME effect in the laminated sample (silver/PVDF/silver) is further verified, which is realized through the coupling of the piezoelectric effect and the Ampere forces caused by the eddy current under the DC bias magnetic field. With the increase of DC magnetic field, the ME voltage induced by the Ampere forces increases linearly at the resonance frequency when the sample is subjected to a specific AC magnetic field. The ME voltage of the sample also shows a strong linear response to the AC magnetic field when subjected to a specific DC magnetic field. As a result, the ME voltage coefficient can be obtained at the resonance frequency, which reaches $\alpha = 299.97$ mV/cm·Oe under the DC magnetic field of 1000 Oe amplitude. Besides, the theoretical model of the ME energy conversion is established, which matches well with the experimental results. Consequently, both AC and DC magnetic field sensing can be realized by observing the ME voltage. Future work will be devoted to the monitoring of the current in the wire, which is expected to be realized by detecting the magnetic field around the wire. With a good linear response and high ME voltage coefficient, the proposed ME composite without requiring the magnetostrictive phase and power supply is promising for the application of online monitoring sensors used in smart grid.

II. SAMPLE AND EXPERIMENT
A. SAMPLE PREPARATION
The selected film was a three-layer composite consisting of a core layer of PVDF and two layers of silver-plated electrodes. The relative permittivity of the polymer PVDF was about 9.5 and the modulus of elasticity was 2500 MPa. The tested sample was cut into a rectangular piece (40 μm in thickness, 40 mm in length, and 10 mm in width), whose edge was then treated to avoid short circuit in the thickness direction. Fig. 1 illustrated the schematic diagram of the tested sample subjected to AC and DC magnetic fields. The AC magnetic field was applied perpendicularly to the surface of the sample, while the DC magnetic field was parallel to the sample's surface.

B. MAGNETOELECTRIC EXPERIMENT
In the experimental set-up for the ME measurement (Fig. 2), the sample was suspended vertically in the air and its top was clamped on a sample holder. Then, the sample holder
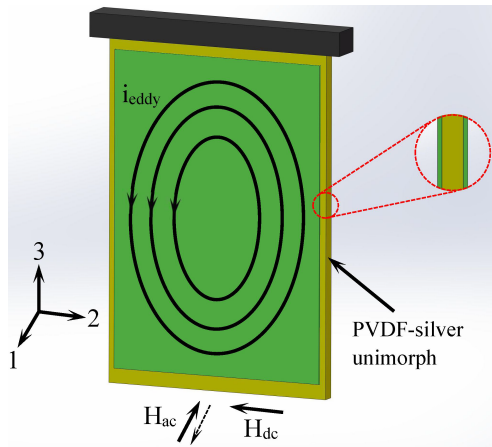
FIGURE 1. Schematic diagram of the tested sample subjected to AC and DC magnetic fields.
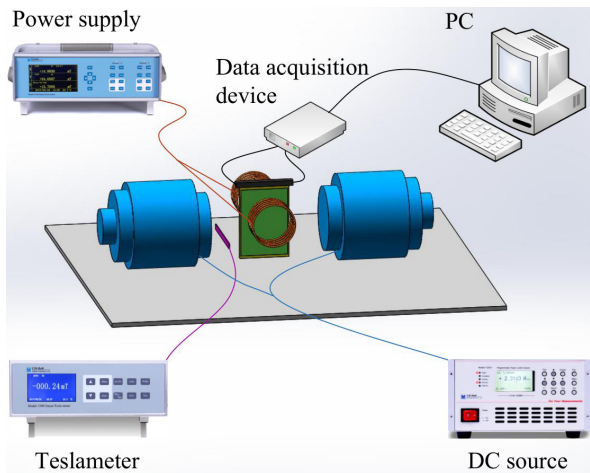

FIGURE 2. Schematic representation of the experimental set-up for the magnetoelectric measurement.

FIGURE 3. Frequency dependence of magnetically induced output voltage from the bender (a) H_{ac} = 6 Oe and (b) H_{ac} = 10 Oe at different H_{dc} values of 800, 1200 and 1600 Oe.

was placed between the poles of an electromagnet driven by a DC source (CH-HALL, Model F2035) which was used to produce the DC magnetic field (H_{dc}), allowing the maximum amplitude to be 3500 Oe. The applied AC magnetic field (h_{ac}) was sinusoidal which could be generated by a Helmholtz coil (maximum amplitude: 30 Oe) connected with a power supply (NJFNKJ, HEAS 20). A teslameter (CH-HALL, Model 1500) was used to measure the values of the magnetic fields. When the AC magnetic field penetrated the laminated sample, eddy currents were thereby induced within the silver electrodes via the Faraday effect. Under the effect of DC bias magnetic field, Ampere forces were generated to act on the piezoelectric phase, resulting in the appearance of the ME voltage. Finally, the output voltage was measured by a data acquisition device (CH-HALL, NET).

III. RESULTS AND DISCUSSION
A. MEASUREMENT OF RESONANCE FREQUENCY
In order to achieve the maximum ME response, the resonance frequency of the measurement system is firstly determined.
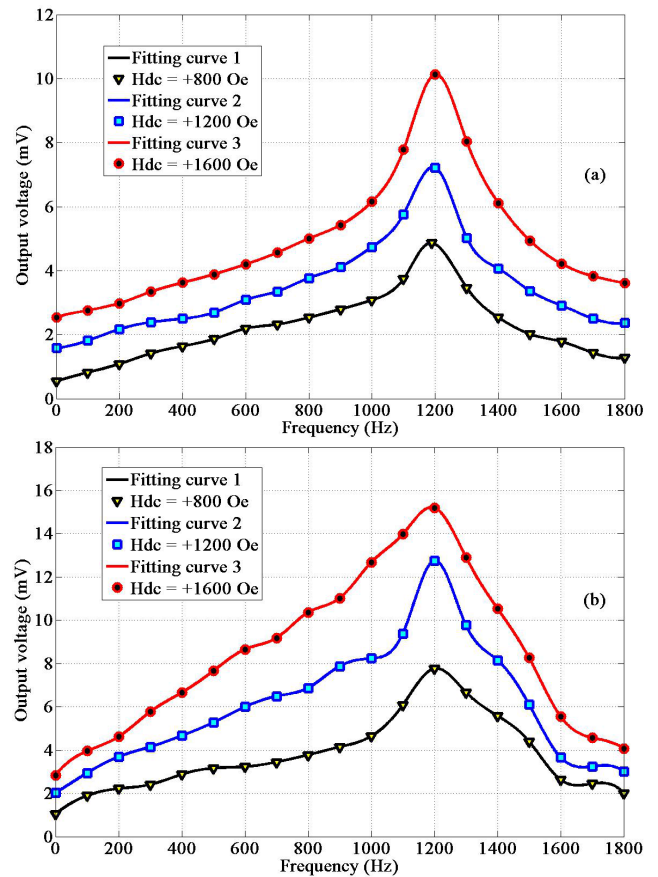
Fig. 3 shows the variations of output voltage versus frequency of the applied AC magnetic field for the prepared sample at different H_{dc} values of 800, 1200 and 1600 Oe, when the applied AC magnetic field amplitude (H_{ac}) is kept at 6 and 10 Oe, respectively. It can be seen from two figures that the six curves exhibit roughly the same change trend, which indicates the reliability of the experimental results. Meanwhile, the six curves reach the peak value at the frequency of about 1200 Hz, so the resonance frequency of the ME system can be obtained as 1200 Hz.

B. MAGNETOELECTRIC RESPONSES
The observed output voltage (V_{out}) in the three-layer composite (silver/PVDF/silver) may be the sum of two distinct contributions: the first one is the parasitic voltage (e_B) generated by the AC magnetic flux (Φ_B) penetrating into the closed contour of the experimental loop, which is composed of two wires connecting the sample with the data acquisition device shown in Fig. 2. According to Faraday's laws, potential difference appears between the electrodes of the sample, which can be expressed as $e_B = -d\Phi_B/dt$. The second contribution may originate from the true ME voltage (V_{ME}) due to the presence of eddy currents within the silver electrodes. When the

surface of the metal electrodes is subjected to an AC magnetic flux $\Phi_{ac} = \iint_A \mu_0 \boldsymbol{h_{ac}} \cdot d\boldsymbol{A}$, where $\boldsymbol{h_{ac}} = H_{ac}\, \boldsymbol{e^{j\omega t}}$ is the AC magnetic induction vector, ω is the angular frequency, μ_0 is the permeability of the silver electrode and A is the loop area in the conductor, the induced electromotive forces (e) appear around the concentric loops via the Faraday's equation: $e = -d\Phi_{ac}/dt = -j\omega\mu_0 A h_{ac}$, leading to the appearance of eddy currents in the electrodes. Under the effect of DC bias magnetic field, Ampere forces are generated and transferred to the piezoelectric layer, resulting in the generation of V_{ME}. By using the superposition theorem, the total V_{out} is written:

$$V_{out} = V_{ME} + e_B \qquad (1)$$

In order to verify the rationality of the above conjectures, ME responses under different conditions are measured. Fig. 4(a) shows the variation of V_{out} versus H_{dc} at the resonance frequency when no AC magnetic field is applied. It can be seen that V_{out} is very weak and has no obvious trend, which can be ignored to a certain extent. Fig. 4(b) indicates the V_{out} as a function of H_{ac} at different H_{dc} values. When no DC bias magnetic field is applied, the piezoelectric contribution to the measured V_{out} is null, the H_{ac} dependence of the measured V_{out} confirms that it is only due to a loop effect and not a ME coupling. It should be emphasized that the e_B always exists owing to the presence of Φ_B, and its magnitude is only related to H_{ac} and the effective area of the closed contour subjected to Φ_B at the resonance frequency. Obviously, the same parasitic effect occurs at H_{dc} value of +200 Oe and the difference between the two curves corresponds to a true ME voltage, which accounts for a large proportion of V_{out}.

In order to further explore the ME coupling and derive the theoretical expression of Ampere forces, the current density $k(r)$ associated with the eddy current should be determined. As we all know, the relationship between induced electromotive force and electric field is as follows: $e = \oint_l \boldsymbol{E(r)} \cdot d\boldsymbol{l}$, where r and l are the radius and circumference of the eddy current loop respectively, $l = 2\pi r$ (here, we approximate the loop as a circle to simplify the formula derivation). Thus, the $k(r)$ at the distance r of the center of the loop can be expressed as:

$$k(r) = \gamma E(r) = \frac{\gamma e}{2\pi r} = \frac{-j\omega\mu_0\gamma r h_{ac}}{2} \qquad (2)$$

where γ is the conductivity of silver. As a result, the eddy currents in each electrode can be obtained by

$$i_{ed} = \oint_l k(r)dl = \oint_l \frac{-j\omega\mu_0\gamma r h_{ac}}{2}dl = -j\omega\mu_0\gamma\pi r^2 h_{ac} \qquad (3)$$

Fig. 4(c) shows the waveforms of true V_{ME} and reference h_{ac} with amplitude of 6 Oe and frequency of 1200 Hz when the sample is subjected to H_{dc} of +200 Oe amplitude. Stable signal conversion between h_{ac} and V_{ME} are evident under the effect of H_{dc}. As it is expected by (3), the frequency of V_{ME} is same as that of h_{ac} due to the frequency consistency of eddy currents i_{ed} and h_{ac}. Besides, the phase angle difference between i_{ed} and h_{ac} in the theoretical derivation is 90°, resulting in the same phase angle difference between V_{ME} and h_{ac}
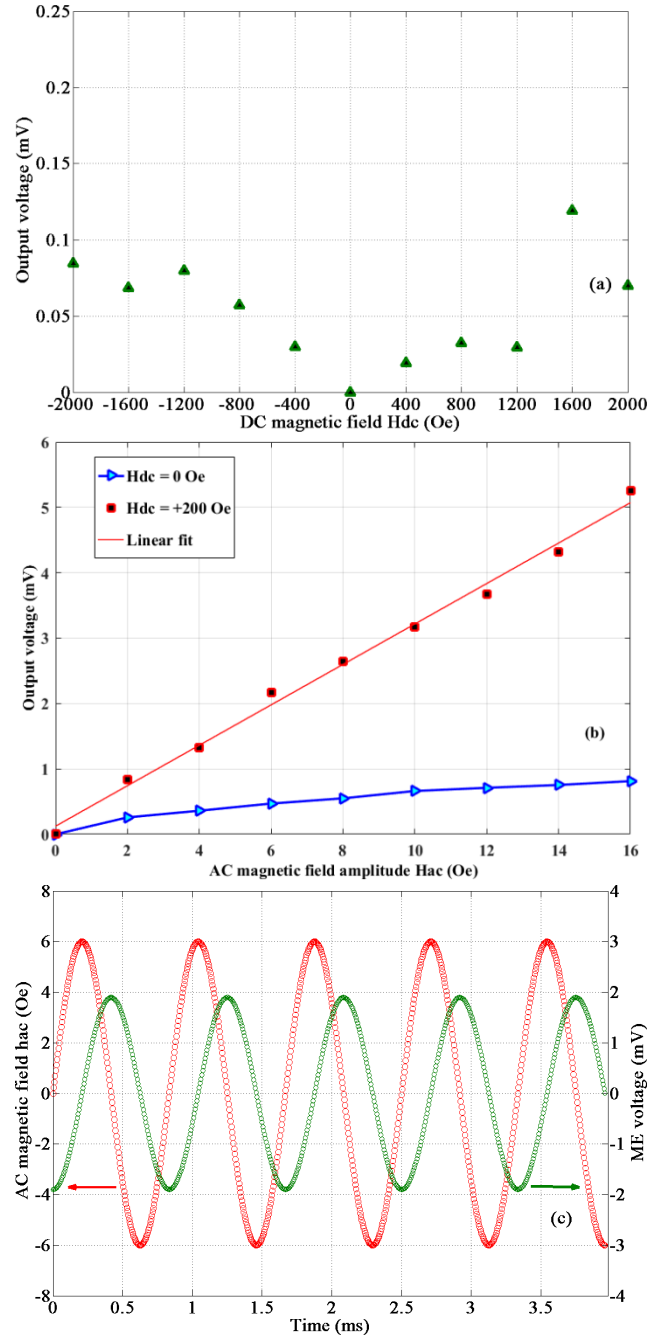

FIGURE 4. (a) Variation of output voltage versus DC bias magnetic field at the resonance frequency when no AC magnetic field is applied and (b) Output voltage as a function of H_{ac} at different H_{dc} values of 0 and +200 Oe and (c) Waveforms of reference AC magnetic field (h_{ac}) with amplitude of 6 Oe and frequency of 1200 Hz and true ME voltage (V_{ME}) when H_{dc} = +200 Oe.

in Fig.4(c). Therefore, the above ME responses can clearly prove that the PVDF unimorph bender has a considerable ME effect, which is mainly due to the appearance of Ampere forces produced by eddy currents.

As illustrated in Fig. 5, the experimental V_{ME} of the sample show strong linear responses to H_{dc} at the resonance frequency when different AC magnetic fields of 2 and 4 Oe
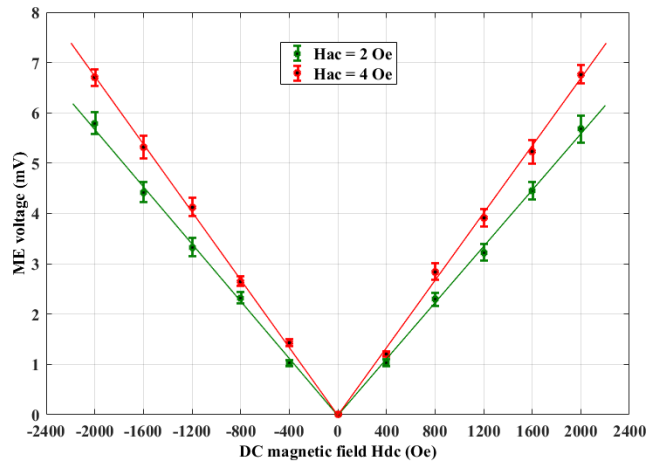
FIGURE 5. Amplitude of ME voltage as a function of applied DC magnetic field for different reference AC magnetic fields at the resonance frequency of 1200 Hz. Error bars represent the standard deviation of at least three independent measurements.
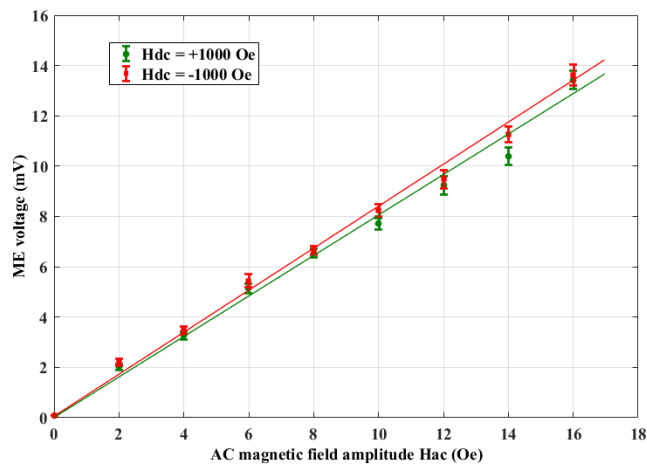
FIGURE 6. Amplitude of ME voltage as a function of AC magnetic field amplitude for different DC magnetic fields at the resonance frequency of 1200 Hz.

amplitude are applied, respectively. This phenomenon can be explained as follows: when eddy currents exist in the silver electrodes, each current loop (L) locally induces an infinitesimal dynamic Ampere force ($d\boldsymbol{F}$) on them which is expressed as the vector product:

$$\mathrm{d}\boldsymbol{F} = i_{ed}(d\boldsymbol{l} \times \boldsymbol{B}) = \mu_0 i_{ed}\left[d\boldsymbol{l} \times (\boldsymbol{H_{dc}} + \boldsymbol{h_{ac}})\right] \quad (4)$$

Since the diameter of the Helmholtz coils is twice larger than that of the sample, a homogeneous magnetic induction may be assumed in the piezoelectric material. Consequently, the global force $\boldsymbol{F} = \int_L d\boldsymbol{F}$ acting on the loop is null but the whole loop undergoes a torque which can be considered as the total torque on each electrode:

$$\begin{aligned} M_1 &= |\boldsymbol{m} \times \boldsymbol{B}| = |i_{ed}\boldsymbol{A} \times \boldsymbol{B}| \\ &= \mu_0 i_{ed}\,|\boldsymbol{A} \times (\boldsymbol{H_{dc}} + \boldsymbol{h_{ac}})| \\ &= -j\omega\mu_0^2\gamma\pi^2 r^4 H_{dc} h_{ac} \end{aligned} \quad (5)$$

where $\boldsymbol{m}$ is the molecular magnetic moment of the eddy current loop.

In the present study, the torques M_1 and M_2 on both electrodes are equal by symmetry since the PVDF film is isotropic in the plane. Thus, the total torque on the sample is expressed as $M_{TOT} = 2M_1$. As previously reported, this is a theoretically expected result when considering the proportionality between an applied external moment and the electrical charges (Q) generated at the electrodes of a piezoelectric unimorph bender [26], [27]:

$$Q = \frac{3d_{31}l}{t^2}M_{TOT} = \frac{-j6d_{31}l\omega\mu_0^2\gamma\pi^2 r^4 H_{dc}h_{ac}}{t^2} \quad (6)$$

where l, t and d_{31} are the length, thickness and transverse piezoelectric coefficient of the sample, respectively. Thus, the corresponding ME voltage caused by Ampere forces may be expressed as:

$$V_{ME} = \frac{Q}{C_p} = \frac{-j6d_{31}l\omega\mu_0^2\gamma\pi^2 r^4 H_{dc}h_{ac}}{t^2 C_p} \quad (7)$$

where C_p is the capacitance of the sample. As expected, this result once again proves that the frequency of applied h_{ac} is equal to the frequency of V_{ME}, and the phase angle difference is 90°, which is consistent with the conclusion in Fig. 4(c).

Finally, the modulus of theoretical ME voltage can be given by

$$|V_{ME}| = \frac{6d_{31}l\omega\mu_0^2\gamma\pi^2 r^4 H_{dc}H_{ac}}{t^2 C_p} \quad (8)$$

By combining (8) and Fig. 5, it can be concluded that with the increase of H_{dc}, the induced Ampere forces and torque gradually become greater, which lead to a linear increase in the magnitude of the ME voltage. Moreover, two curves present a marked minimum of the ME voltage at a same DC magnetic field value ($H_{dc} = 0$) corresponding to the phase switching value. Thus, DC magnetic field measurement can be realized by measuring the V_{ME} of the laminated sample (silver/PVDF/silver) when it is subjected to a specific H_{ac}.

In order to further explore the ME response of the laminated sample when the H_{ac} is changed, the variation of V_{ME} versus the applied H_{ac} is then measured. As illustrated in Fig. 6, the V_{ME} increases linearly with the H_{ac}. Meanwhile, two curves show an approximate linear relation of V_{ME} versus H_{ac} within its dynamic range of 0-16 Oe at different H_{dc} values of +1000 Oe and -1000 Oe. According to (3), it may be explained by the fact that the eddy currents induced within the silver electrodes are significantly stronger due to the increase of H_{ac}. Under the DC bias magnetic field, the corresponding ME response induced by the increased Ampere forces is notably enhanced by using (4), (5) and (7). Consequently, AC magnetic field measurement can be realized by measuring the V_{ME} of the laminated sample when it is subjected to a specific H_{dc}. In this paper, the AC magnetic field originates from the applied AC current in a Helmholtz coil. Thus, the change of current in the wire can be accurately monitored by measuring the ME voltage. In practical application, the
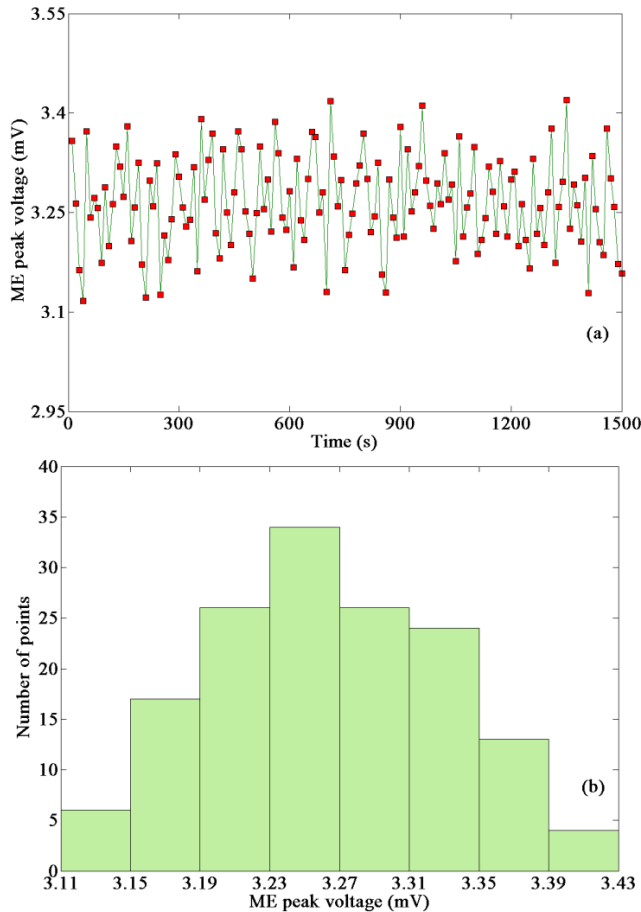
FIGURE 7. ME peak voltage as a function of time and (b) Histogram for voltage distribution when the amplitude of AC magnetic field is 4 Oe at DC magnetic field value of 1000 Oe.

wire can also be made into current-carrying coil to replace the Helmholtz coil in the device.

With the purpose of confirming the reliability of measurement results, the accuracy of the ME measurement system has been investigated. Fig. 7(a) shows the ME peak voltage as a function of time when the H_{ac} is 4 Oe at H_{dc} values of +1000 Oe. The accuracy (A_n) of the ME system can be calculated by

$$A_n = \nu + \varepsilon \qquad (9)$$

where ν is the systematic error, and ε is the uncertainty. In Fig. 7(a), the arbitrary measured voltages V_i and V_j satisfy

$$|V_i - V_j| < 2\sigma \qquad (10)$$

where σ is the standard deviation. Therefore, the systematic error can be ignored in the experiments. Fig. 7(b) indicates the histogram for the peak voltage distribution. It can be considered that the voltages obey normal distribution to a certain extent. The uncertainty is calculated by

$$\varepsilon = \pm 4\sigma/\sqrt{n} \qquad (11)$$

where n is the number of measurements ($n = 150$). Hence, the accuracy of the sensor $A_n = \varepsilon = \pm 0.0562$ mV.
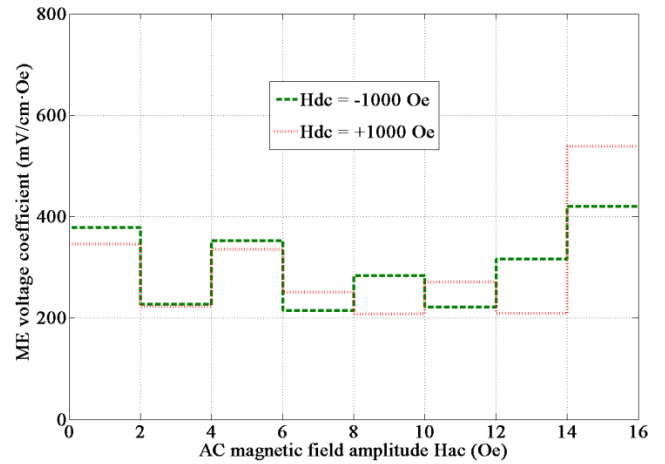

FIGURE 8. Variation of the ME voltage coefficient of the proposed composite in the adjacent region with AC magnetic field interval of 2 Oe when the amplitude of DC magnetic field is 1000 Oe.

TABLE 1. Comparison between ME voltage coefficients of different materials.

Types	Materials	α mV/cm • Oe
Single phase samples	Cr$_2$O$_3$ crystal @1 kHz [28]	20
	Charged PVC @1 kHz [29]	178
Particulate composite samples	P(VDF-TrFE)+72wt% CoFe$_2$O$_4$ @5 kHz [30]	40
	P(VDF-TrFE)+20 wt% δ-FeO(OH) @7 kHz [31]	0.4
Multilayer samples	Terfenol-D/BNKT-BT/Terfenol-D @1 kHz [32]	40.7
	PZT/Alumina @4.9 kHz [23]	79
	silver/PVDF/silver @1 kHz [This work]	299.97
	PU+2wt% Fe$_3$O$_4$/PVDF/PU+2 wt% Fe$_3$O$_4$ @1 kHz [33]	753.3

In practical application, an offset might be added to the output side of the sensor to insure the accuracy. Generally, the offset mainly depends on the output characteristics and working environment of the sensor.

Based on the measured ME results, the ME voltage coefficient α can be calculated as follows:

$$\alpha = \frac{\delta E}{\delta H_{ac}} = \frac{1}{t}\left(\frac{\delta V_{ME}}{\delta H_{ac}}\right) \qquad (12)$$

Fig. 8 shows the variation of the ME voltage coefficient of the proposed composite in the adjacent region with AC magnetic field interval of 2 Oe. It can be clearly seen that most of the data on the two polylines are between 200 and 400 mV/cm·Oe when the applied H_{dc} is +1000 and -1000 Oe, respectively. As a result, ME voltage coefficient can be

obtained by calculating the average value of two polylines, which reaches $\alpha = 299.97$ mV/cm·Oe at the resonance frequency. The Table 1 presents a comparison of ME voltage coefficients of silver/PVDF/silver composite with those obtained from other literatures. It can be seen that the multilayer composites show larger ME voltage coefficients compared to the particulate composites and single phase samples. Although obtained ME voltage coefficient in this work is probably not high enough, a considerable ME effect is very promising for the application of multifunctional sensors due to its high cost performance.
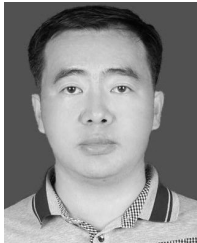
IV. CONCLUSION

In this paper, we focused on investigating the ME coupling effect within a three-layer ME composite consisting of a core layer of PVDF and two layers of silver-plated electrodes. The existence of ME effect in the laminated sample (silver/PVDF/silver) is further verified, which is realized through the coupling of the piezoelectric effect and the Ampere forces caused by the eddy current under the DC bias magnetic field. With the increase of DC magnetic field, the ME voltage induced by the Ampere forces increases linearly at the resonance frequency when the sample is subjected to a specific AC magnetic field. The ME voltage of the sample also shows a strong linear response to the AC magnetic field when subjected to a specific DC magnetic field. As a result, the ME voltage coefficient can be obtained at the resonance frequency, which reaches $\alpha = 299.97$ mV/cm·Oe under the DC magnetic field of 1000 Oe amplitude. Besides, the theoretical model of the ME energy conversion is established, which matches well with the experimental results. The characteristics of this ME composite are summarized as follows: 1) Without requiring the magnetostrictive phase and power supply, the three-layer composite still produces a considerable ME effect; 2) With a good linear response, high ME voltage coefficient can be obtained at the resonance frequency. 3) Both AC and DC magnetic field sensing can be realized by observing the ME voltage. Apparent ME response and low-cost structure of such multifunctional composite are promising for the application of online monitoring sensors used in smart grid technologies.

REFERENCES

[1] E. U. Ogbodo, D. Dorrell, and A. M. Abu-Mahfouz, "Cognitive radio based sensor network in smart grid: Architectures, applications and communication technologies," *IEEE Access*, vol. 5, pp. 19084–19098, 2017.

[2] W. Wang and Z. Lu, "Cyber security in the smart grid: Survey and challenges," *Comput. Netw.*, vol. 57, no. 5, pp. 1344–1371, Apr. 2013.

[3] A. Bernieri, L. Ferrigno, M. Laracca, and A. Rasile, "An AMR-based three-phase current sensor for smart grid applications," *IEEE Sensors J.*, vol. 17, no. 23, pp. 7704–7712, Dec. 2017.

[4] Y. Saleem, N. Crespi, M. H. Rehmani, and R. Copeland, "Internet of Things-aided smart grid: Technologies, architectures, applications, prototypes, and future research directions," *IEEE Access*, vol. 7, pp. 62962–63003, 2019.

[5] M. Zhang, K. Chow, and P. Chong, "Optical fibre-based environmental sensors utilizing wireless smart grid platform," in *Proc. Smart Grid Inspired Future Technol.*, London, U.K., Aug. 2017, pp. 253–258.

[6] B. Pan, P. Zeng, and K. K. R. Choo, "A new multidimensional and fault-Tolerable data aggregation scheme for privacy-preserving smart grid communications," in *Proc. Int. Conf. Appl. Techniq. Cyber Secur. Intell.*, Ningbo, China, Oct. 2017, pp. 206–219.

[7] R. Zhang, "Application of optical fiber sensors in smart grid," in *Proc. Int. Conf. Opt. Instrum. Technology: Opt. Sensors Appl.*, Beijing, China, Nov. 2013, pp. 1–6.

[8] C. Q. Lin, H. Tong, W. F. Yu, Y. C. Xin, and R. F. Zhang, "Distribution grid intelligent state monitoring and fault handling platform based on ubiquitous power Internet of Things," *J. N. E. Elect. Power Univ.*, vol. 39, no. 4, pp. 1–4, Aug. 2019.

[9] M. Park, S. Byun, W. Kim, J. Lee, K. Choi, and H. Lee, "Non-contact measurement of current distribution in parallel conductors by using Hall sensors," *IEEE Trans. Appl. Supercond.*, vol. 18, no. 2, pp. 1135–1138, Jun. 2008.

[10] Y. Liu, F. Lin, Q. Zhang, and H. Zhong, "Design and construction of a Rogowski coil for measuring wide pulsed current," *IEEE Sensors J.*, vol. 11, no. 1, pp. 123–130, Jan. 2011.

[11] R. Morello, S. C. Mukhopadhyay, Z. Liu, D. Slomovitz, and S. R. Samantaray, "Advances on sensing technologies for smart cities and power grids: A review," *IEEE Sensors J.*, vol. 17, no. 23, pp. 7596–7610, Dec. 2017.

[12] P. Martins and S. Lanceros-Méndez, "Polymer-based magnetoelectric materials," *Adv. Funct. Mater.*, vol. 23, no. 27, pp. 3371–3385, Aug. 2013.

[13] J. Jin, F. Zhao, K. Han, M. A. Haque, L. Dong, and Q. Wang, "Multiferroic polymer laminate composites exhibiting high magnetoelectric response induced by hydrogen-bonding interactions," *Adv. Funct. Mater.*, vol. 24, no. 8, pp. 1067–1073, Sep. 2014.

[14] J. Zhang, P. Li, Y. Wen, W. He, A. Yang, C. Lu, J. Qiu, J. Wen, J. Yang, Y. Zhu, and M. Yu, "High-resolution current sensor utilizing nanocrystalline alloy and magnetoelectric laminate composite," *Rev. Sci. Instrum.*, vol. 83, no. 11, Nov. 2012, Art. no. 115001.

[15] C. W. Nan, M. I. Bichurin, S. X. Dong, D. Viehland, and G. Srinivasan, "Multiferroic magnetoelectric composites: Historical perspective, status, and future directions," *J. Appl. Phys.*, vol. 103, no. 3, Feb. 2008, Art. no. 031101.

[16] L. Chen, P. Li, and Y. Wen, "Enhanced magnetoelectric effects in laminate composites of Terfenol-D/Pb(zr, TiO)$_3$ with high-permeability FeCuNbSiB ribbon," *Smart Mater. Struct.*, vol. 19, no. 11, Aug. 2010, Art. no. 115003.

[17] J. Ryu, A. V. Carazo, K. Uchino, and H.-E. Kim, "Magnetoelectric properties in piezoelectric and magnetostrictive laminate composites," *Jpn. J. Appl. Phys.*, vol. 40, no. Part 1, No. 8, pp. 4948–4951, Aug. 2001.

[18] J. van den Boomgaard and R. A. J. Born, "A sintered magnetoelectric composite material BaTiO$_3$-Ni(Co, Mn) Fe$_2$O$_4$," *J. Mater. Sci.*, vol. 13, no. 7, pp. 1538–1548, Jul. 1978.

[19] M. Bichurin, R. Petrov, V. Leontiev, G. Semenov, and O. Sokolov, "Magnetoelectric current sensors," *Sensors*, vol. 17, no. 6, pp. 1271–1283, May 2017.

[20] C. Ming Leung, S. Wing Or, and S. L. Ho, "High current sensitivity and large magnetoelectric effect in magnetostrictive–piezoelectric concentric ring," *J. Appl. Phys.*, vol. 115, no. 17, May 2014, Art. no. 17A933.

[21] J. Zhang, J. Wul, Q. Yang, X. Wang, X. Zheng, and L. Cao, "An autonomous current-sensing system for electric cord monitoring using magnetoelectric sensors," in *Proc. IEEE Int. Electr. Mach. Drives Conf. (IEMDC)*, Miami, FL, USA, May 2017, pp. 1–5.

[22] H. Liu, X. Sun, Y. Gao, H. Wang, and Z. Gao, "Magnetostrictive and kinematic model considering the dynamic hysteresis and energy loss for GMA," *Chin. J. Mech. Eng.*, vol. 30, no. 2, pp. 241–255, Mar. 2017.

[23] B. Guiffard, D. Guyomar, L. Garbuio, R. Belouadah, J. Zhang, and P. J. Cottinet, "Eddy current induced magnetoelectricity in a piezoelectric unimorph bender," *Appl. Phys. Lett.*, vol. 96, no. 4, Jan. 2010, Art. no. 044105.

[24] F. Wang, X. Zhao, and J. Li, "PVDF energy-harvesting devices: Film preparation, electric poling, energy-harvesting efficiency," in *Proc. IEEE Conf. Electr. Insul. Dielectr. Phenomena (CEIDP)*, Ann Arbor, MI, USA, Oct. 2015, pp. 1–4.

[25] N. Castro, S. Reis, M. P. Silva, V. Correia, S. Lanceros-Mendez, and P. Martins, "Development of a contactless DC current sensor with high linearity and sensitivity based on the magnetoelectric effect," *Smart Mater. Struct.*, vol. 27, no. 6, Jun. 2018, Art. no. 065012.

[26] Q.-M. Wang, X.-H. Du, B. Xu, and L. E. Cross, "Theoretical analysis of the sensor effect of cantilever piezoelectric benders," *J. Appl. Phys.*, vol. 85, no. 3, pp. 1702–1712, Feb. 1999.

[27] J. G. Smits and W. Choi, "The constituent equations of piezoelectric heterogeneous bimorphs," *IEEE Trans. Ultrason., Ferroelectr., Freq. Control*, vol. 38, no. 3, pp. 256–270, May 1991.

[28] D. Guyomar, B. Guiffard, R. Belouadah, and L. Petit, "Two-phase magnetoelectric nanopowder/polyurethane composites," *J. Appl. Phys.*, vol. 104, no. 7, Aug. 2008, Art. no. 074902.

[29] J. W. Zhang, R. Belouadah, L. Lebrun, and D. Guyomar, "Magnetoelectric phenomena of insulator polymers after corona poling: Procedure and experiments," *Sens. Actuators A, Phys.*, vol. 220, pp. 112–117, Sep. 2014.

[30] P. Martins, R. Gonçalves, S. Lanceros-Mendez, A. Lasheras, J. Gutiérrez, and J. M. Barandiarán, "Effect of filler dispersion and dispersion method on the piezoelectric and magnetoelectric response of CoFe$_2$O$_4$/P(VDF-TrFE) nanocomposites," *Appl. Surf. Sci.*, vol. 313, pp. 215–219, May 2014.

[31] P. Martins, A. Larrea, R. Gonçalves, G. Botelho, E. V. Ramana , S. K. Mendiratta, V. Sebastian, and S. Lanceros-Mendez, "Novel Anisotropic Magnetoelectric Effect on d-FeO(OH)/P(VDF-TrFE) Multiferroic Composites," *ACS Appl. Mater. Interface*, vol. 7, no. 21, pp. 11224–11229, May 2015.

[32] Y. Jia, S. W. Or, J. Wang, H. L. W. Chan, X. Zhao, and H. Luo, "High magnetoelectric effect in laminated composites of giant magnetostrictive alloy and lead-free piezoelectric ceramic," *J. Appl. Phys.*, vol. 101, no. 10, May 2007, Art. no. 104103.

[33] R. Belouadah, D. Guyomar, B. Guiffard, and J.-W. Zhang, "Phase switching phenomenon in magnetoelectric laminate polymer composites: Experiments and modeling," *Phys. B, Condens. Matter*, vol. 406, no. 14, pp. 2821–2826, Apr. 2011.

YUDONG ZHANG received the B.S. degree in transmission engineering from Northeast Electric Power University, Jilin, China, in 2018, where he is currently pursuing the M.S. degree in electrical engineering with the School of Electrical Engineering. His current research interests include functional magnetoelectric materials and magnetoelectric sensors.

BING QI received the Ph.D. degree in plasma physics from the Dalian University of Technology, Dalian, China, in 2007. He is currently an Associate Professor of high-voltage and insulation technology with Northeast Electric Power University. His current research interests include partial discharge diagnosis and numerical simulation of atmospheric pressure plasma.

TAIPING YAO received the B.S. degree in applied chemistry from Northeast Electric Power University, Jilin, China, in 2018, where he is currently pursuing the M.S. degree in electrical engineering. His current research interest includes dielectric insulation materials.

• • •